J. Fluid Mech. (1999), *vol.* 396, *pp.* 319–344. Printed in the United Kingdom

On the causal behaviour of flow over an elastic wall

By R. J. LINGWOOD[1] AND N. PEAKE[2]

[1] Department of Engineering, University of Cambridge, Trumpington Street, Cambridge CB2 1PZ, UK

[2] Department of Applied Mathematics and Theoretical Physics, University of Cambridge, Silver Street, Cambridge CB3 9EW, UK

(Received 14 May 1998 and in revised form 17 May 1999)

In this paper we consider the causal response of the inviscid shear-layer flow over an elastic surface to excitation by a time-harmonic line force. In the case of uniform flow, Brazier-Smith & Scott (1984) and Crighton & Oswell (1991) have analysed the long-time limit of the response. They find that the system is absolutely unstable for sufficiently high flow speeds, and that at lower speeds there exist certain anomalous neutral modes with group velocity directed towards the driver (in contradiction of the usual radiation condition of out-going disturbances). Our aim in this paper is to repeat their analysis for more realistic shear profiles, and in particular to determine whether or not the uniform-flow results can be regained in the limit in which the shear-layer thickness on a length scale based on the fluid loading, denoted ϵ, becomes small. For a simple broken-line linear shear profile we find that the results are qualitatively similar to those for uniform flow. However, for the more realistic Blasius profile very significant differences arise, essentially due to the presence of the critical layer. In particular, we find that as $\epsilon \to 0$ the minimum flow speed required for absolute instability is pushed to considerably higher values than was found for uniform flow, leading us to conclude that the uniform-flow problem is an unattainable singular limit of our more general problem. In contrast, we find that the uniform-flow anomalous modes (written as $\exp(\mathrm{i}kx - \mathrm{i}\omega t)$, say) do persist for non-zero shear over a wide range of ϵ, although now becoming non-neutral. Unlike the case of uniform flow, however, the k-loci of these modes can now change direction more than once as the imaginary part of ω is increased, and we describe the connection between this behaviour and local properties of the dispersion function. Finally, in order to investigate whether or not these anomalous modes might be realizable at a finite time after the driver is switched on, we evaluate the double Fourier inversion integrals for the unsteady flow numerically. We find that the anomalous mode is indeed present at finite time, once initial transients have propagated away, not only for impulsive start-up but also when the forcing amplitude is allowed to grow slowly from a small value at some initial instant. This behaviour has significant implications for the application of standard radiation conditions in wave problems with mean flow.

1. Introduction

The unsteady behaviour of the flow over elastic and compliant surfaces has received considerable attention, due not only to its relevance to situations in which a structure interacts with the surrounding fluid (with applications ranging from naval engineering

to the biodynamics of blood flow), but due also to the occurrence of a range of unusual phenomena of fundamental interest. Some of the earliest work was conducted by Benjamin (1960, 1963) and Landahl (1962), who considered the properties of the linear waves present in the boundary-layer flow over an elastic plate in two dimensions. A particular feature of their analysis was the classification of the wave energy of the system, and in particular they showed that negative-energy waves can be present. Since then, the issue has been investigated in detail by Cairns (1979), and studies for more general types of elastic material have been completed by Carpenter & Garrad (1985, 1986) and Yeo & Dowling (1987).

In parallel to this activity, the simplified problem in which the steady mean flow over the plate is uniform, with the unsteady flow driven by a harmonic line force, has received some attention. This has been completed by Brazier-Smith & Scott (1984) and subsequently by Crighton & Oswell (1991), both using the techniques developed by Briggs (1964) and Bers (1983) for determining the long-time limit of the causal solutions of initial-value problems. Brazier-Smith & Scott were able to show that as well as the negative-energy waves identified by Landahl and Benjamin, the uniform-flow case also has two other unusual features. First, provided that the uniform flow speed is larger than a critical value, the flow is absolutely unstable. Second, below this critical flow speed there exists a neutral mode (written as $\exp(\mathrm{i}kx - \mathrm{i}\omega t)$ say) whose locus moves downwards from the real k-axis as $\mathrm{Im}(\omega)$ is increased from zero, before turning round once and reaching infinity through the upper half-plane. Crighton & Oswell investigated this second point in some detail, and were able to interpret this anomalous behaviour as corresponding to a mode located downstream of the driver but with its group velocity directed upstream, i.e. towards the driver, contrary to the usual Rayleigh–Lighthill criterion (Lighthill 1960) of outgoing group velocity at infinity. This anomalous propagation has also been identified in a number other systems, such as in the related problem of flow over membranes (Kelbert & Sazonov 1996), capillary waves in jets (Leib & Goldstein 1986) and in the propagation of certain modes in swirling duct flow (Golubev & Atassi 1997).

Abrahams & Wickham (1994) argue that the Brazier-Smith & Scott (1984) and Crighton & Oswell (1991) model of uniform flow over an infinitely long plate in two dimensions is not sufficiently realistic, and that the predicted absolute instability and anomalous propagation cannot therefore be observed in an experiment. For instance, the effects of finite plate length have been considered by Lucey & Carpenter (1992, 1993), Wu & Maestrello (1995) and Lucey (1998), and it seems that these results differ significantly from Crighton & Oswell's infinite-span behaviour. Moreover, Peake (1997) used Crighton & Oswell's approach to investigate the effects of transverse plate stiffness, by analysing the wave properties of a circular cylinder with uniform axial flow forced by a harmonic ring source. In the limit of very large cylinder radius Crighton & Oswell's results are regained, but it was seen that both the absolute instability and the anomalous propagation are lost as the cylinder radius is decreased. Indeed, for 2 cm thick steel in water at a moderate mean flow speed the cylinder radius has to be in excess of 3.3 km in order to observe the anomalous-propagation mode, while the absolute-instability boundary is also pushed to unrealistically high levels.

In this paper we aim to extend the uniform-flow model in a different way, by investigating the effects of including a genuine boundary-layer flow over the plate. In other words, we will revisit the model first studied by Benjamin (1960, 1963) and Landahl (1962), but now investigating the possibility of absolute instability and anomalous propagation. We note that absolute instability was detected in this problem

by Carpenter & Garrad (1986), but our aim here will be to conduct a more detailed study, and in particular to relate our results for very thin shear layers to the earlier results from the uniform-flow calculations. For a given steady shear-layer profile, there are in fact two important dimensionless quantities, namely the normalized flow speed far from the plate, U, and the shear-layer thickness normalized with respect to a length scale based on the fluid loading, ϵ. In the present study we propose to determine whether or not the uniform-flow results are regained from the genuine shear-layer calculations in the limit $\epsilon \to 0$.

In § 2 of this paper we present the mathematical formulation of our problem, in a form that will facilitate direct comparison with Brazier-Smith & Scott and Crighton & Oswell's results. In § 3 we study the existence of absolute instability, first for a simple broken-line model profile (for which the dispersion relation is available analytically), and then for the genuine Blasius flow. Results for the broken-line profile will be seen to be qualitatively similar to those found for uniform flow, although interestingly the absolute instability boundary moves to lower values of U for a range of ϵ. However, we argue that this simple profile is not at all representative of typical behaviour, since it does not possess a critical layer. In fact, the results for the Blasius profile will be shown to be very different from the uniform-flow case, and in particular we find that as $\epsilon \to 0$ the absolute instability boundary is forced to considerably higher values of U than was found by Crighton & Oswell. This demonstrates that the uniform flow is in fact a singular, and unattainable, limit of our more general problem. This is in contrast to the conclusion of Peake (1997) for axial flow past a cylindrical shell, in which Crighton & Oswell's (1991) behaviour was recovered for sufficiently large, but finite, cylinder radius.

In § 4 we investigate the existence of anomalous-propagation modes, and again find modes whose spatial location cannot be correctly predicted by consideration of their local group velocity. Indeed, we also find a mode that could be termed 'doubly anomalous', in that its locus in the spatial plane turns round *twice* before reaching infinity. By evaluating the double Fourier inversion integrals numerically for finite times, we demonstrate in § 5 that the anomalous-propagation modes are not merely a singular feature of taking the long-time limit in the Briggs–Bers method, but can clearly be seen in the flow at finite times once initial transients have been convected away. We find this to be the case not only when the forcing is switched on impulsively at $t = 0$ and kept at constant amplitude, but also when its amplitude is allowed to grow very slowly indeed from a small value at $t = 0$. Concluding remarks are given in § 6.

2. Formulation and solution – inviscid analysis

2.1. *Governing equations*

We consider a thin elastic plate of mass per unit area m_* and bending stiffness B_* (in what follows a suffix $_*$ denotes dimensional variables), which is of infinite extent and which in its undisturbed position lies in the (x_*, z_*)-plane, as shown in figure 1. Fluid of density ρ_* lies above the plate in $y_* > 0$, and for definiteness we will suppose that there is a vacuum in $y_* < 0$, although the presence of fluid here as well could easily be included in our analysis. We suppose that the steady fluid flow above the plate is parallel, and is purely in the x_*-direction with speed $U_* f(y_*/l_*)$. The velocity profile $f(y_*/l_*)$ obeys the zero normal-velocity boundary condition on the undisturbed plate, and $f \to 1$ as $y_*/l_* \to \infty$. Mostly, we will also suppose that $f(0) = 0$ in order to satisfy

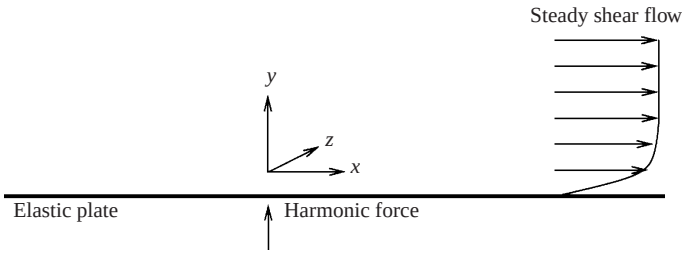

FIGURE 1. The elastic plate with shear flow.

the steady no-slip condition, although this condition will be relaxed at various points in our analysis in order to make comparisons with earlier work. It then follows that U_* is the free-stream flow speed far away from the plate, and l_* is the characteristic (transverse) length scale of the shear flow. We will be taking $f(y_*/l_*)$ to be the Blasius profile, but some preliminary analysis with a simple broken-line profile will also be described, as will some work on a profile representing continuous variation between the Blasius solution and uniform flow.

We wish to consider purely two-dimensional unsteady motion, and we therefore suppose that the plate is subjected to an infinitely long line force lying along the z_*-axis with uniform strength $F_*(t_*)$ per unit length acting in the y_*-direction, which is switched on at time $t_* = 0$ so that $F_*(t_*) = 0$ for $t_* < 0$. Assuming that the forcing is weak, the motion of the plate is linear and is described by the simple thin-shell equation (Junger & Feit 1986, p. 210). In order to obtain results that can be compared with Crighton & Oswell's (1991) uniform-flow analysis, we now non-dimensionalize all lengths by m_*/ρ_* (which is a characteristic length scale based on the fluid loading) and time by $m_*^{5/2}/(\rho_*^2 B_*^{1/2})$. The plate equation then takes the form

$$\frac{\partial^2 \eta}{\partial t^2} + \frac{\partial^4 \eta}{\partial x^4} = F(t)\delta(x) - p(x, 0, t), \tag{2.1}$$

where $\eta(x,t)$ is the transverse plate displacement and $U = U_* m_*^{3/2}/(\rho_* B_*^{1/2})$ is the non-dimensional free-stream speed. The term $p(x,y,t)$ is the hydrodynamic pressure on the plate, and corresponds to the unsteady loading exerted by the fluid.

The unsteady fluid motion is taken to be incompressible and inviscid, and is governed by the linearized Euler equations together with the boundary conditions of continuity of normal velocity at the (moving) wall and zero disturbance at infinity. In order to solve the system we introduce Fourier transforms, with for instance

$$\overline{\eta}(k,\omega) \equiv \int_{-\infty}^{\infty}\int_{-\infty}^{\infty} \eta(x,t)\exp(\mathrm{i}\omega t - \mathrm{i}kx)\mathrm{d}x\,\mathrm{d}t, \tag{2.2}$$

with the overbar denoting transformed variables. The unsteady flow is then described by Rayleigh's equation (e.g. Drazin & Reid 1981), which takes the non-dimensional form

$$(kUf - \omega)\left[\frac{\partial^2 \overline{\phi}}{\partial y^2} - k^2\overline{\phi}\right] - \frac{kU}{\epsilon^2} f''\overline{\phi} = 0. \tag{2.3}$$

Here $\overline{\phi}(y;k,\omega)$ is the transform of the unsteady perturbation to the steady-flow streamfunction, $\epsilon = l_*\rho_*/m_*$ is the ratio of the transverse length scale of the steady shear layer to the fluid-loading length scale, and primes denote differentiation with respect to y/ϵ, and we again emphasize that $f = f(y/\epsilon)$ is the steady shear-layer

profile. The hydrodynamic pressure can be related to the streamfunction via the transform of the linearized x-momentum equation, i.e.

$$\frac{\partial\overline{\phi}}{\partial y}(kUf-\omega)-\frac{\overline{\phi}}{\epsilon}kUf'=-k\overline{p}. \tag{2.4}$$

The zero normal-velocity boundary condition on the plate is evaluated on $y=0$ in our linearized system, and it follows that

$$-k\overline{\phi}(0;k,\omega)=-(\omega-kUf(0))\overline{\eta}(k,\omega). \tag{2.5}$$

By combining (2.5) with (2.4) and the transform of (2.1), we find the effective plate boundary condition in the form

$$\overline{\phi}(0;k,\omega)\left[\frac{k(\omega^2-k^4)}{Ukf(0)-\omega}+\frac{Uf'(0)}{\epsilon}\right]=\frac{\partial\overline{\phi}(0;k,\omega)}{\partial y}\left[\frac{Ukf(0)-\omega}{k}\right]. \tag{2.6}$$

Equations (2.3) and (2.6), together with the free-stream boundary condition that $\overline{\phi}(y;k,\omega)\to 0$ as $y\to\infty$, define an eigenvalue problem for either ω or k, the solution of which will be described in due course. The full solution of the problem, however, must be determined by inverting the Fourier transforms, with for instance

$$\eta(x,t)=\frac{1}{4\pi^2}\int_C\int_{-\infty}^{\infty}\frac{|k|\overline{F}_0(\omega)}{D(k,\omega)}\exp(\mathrm{i}kx-\mathrm{i}\omega t)\mathrm{d}k\,\mathrm{d}\omega, \tag{2.7}$$

where $|k|=\pm k$ for $\mathrm{Re}\,(k)$ positive and negative, respectively, $\overline{F}_0(\omega)$ is the time Fourier transform of the line forcing and $D(k,\omega)$ is the dispersion function. In general, the dispersion function can only be determined numerically, apart from in the case of particularly simple model profiles. The inversion contours in (2.7) are chosen to satisfy causality – the temporal contour C is chosen to be sufficiently high in the ω-plane to lie above all singularities of $D(k,\omega)$ (note that because the forcing is switched on at $t=0$, $\overline{F}_0(\omega)$ is analytic in the upper half of the ω-plane), so that $\eta(x,t)=0$ for $t<0$, and the spatial contour is chosen in the first instance to lie along the real k-axis.

2.2. *Determination of long-time limit*

The plate displacement at arbitrary $t>0$ could now be determined by solution of (2.3) and (2.6) to yield values of $D(k,\omega)$, together with numerical evaluation of the double inversion integral in (2.7), and indeed the results of such a calculation will be described in § 5 in the simple case of uniform flow (for which an analytical expression for the dispersion function is available). However, in general it proves much more convenient, and indeed more illuminating, to consider the behaviour of the system in the limit $t\to\infty$. In order to do this we follow exactly the procedure used in Brazier-Smith & Scott (1984) and Crighton & Oswell (1991), and apply the technique developed first by Briggs (1964) and later by Bers (1984) for determining the causal long-time behaviour of initial-value problems. The idea is to deform the temporal contour C continuously downwards towards the real ω-axis, while simultaneously deforming the spatial contour off the real k-axis so that the contour is never crossed by any poles of the integrand (i.e. solutions of the dispersion relation $D(k,\omega)=0$) in the k-plane, or by any spatial branch points. A number of different types of behaviour are possible, but in the first instance we need only consider two possibilities.

First, as C is deformed downwards two poles in the k-plane move together from opposite sides of the contour, and if these poles merge and 'pinch' the spatial contour before C has moved onto the real ω-axis then the deformation must stop – say this

happens for $\omega = \omega_0$ and $k = k_0$. It is shown very clearly by Brazier-Smith & Scott (1984) that the long-time response is then dominated by a contribution from the pinch point, and indeed that the response is proportional to $\exp(\mathrm{i}k_0 x - \mathrm{i}\omega_0 t)$ as $t \to \infty$. Since $\mathrm{Im}(\omega_0)$ is necessarily positive in this case, it follows that the response grows exponentially in time for all x, and therefore the flow is absolutely unstable. It is clear that at the pinch point $\partial\omega/\partial k = 0$, and to identify absolute instability we therefore need to look for saddle points of the dispersion function $D(k, \omega)$ in the k-plane. However, it must be noted that not every saddle point of the dispersion function can give rise to an absolute instability, and as is made clear by the above argument it is also necessary for the saddle to be formed as a result of modes merging from opposite half-planes. The occurrence of absolute instability in our system will be described in § 3.

Second, if no such pinching occurs before C moves onto the real ω-axis then it follows that the flow cannot be absolutely unstable (but note that marginally stable saddle points can still arise with $\mathrm{Im}(\omega_0) = 0$). In this case the long-time behaviour will be dominated by the free modes of the system for real ω (so if for instance $F(t) = \exp(-\mathrm{i}\omega_f t)H(t)$, with $H(t)$ being the unit step function, then the response will be dominated by spatial modes with wavenumbers satisfying $D(k, \omega_f) = 0$). The question of whether these modes are located either upstream or downstream of the driver is answered by considering in which half of the k-plane the mode originated from before C was deformed. The spatial contour must be deformed below modes originating in the upper half of the k-plane as C moves downwards, so that those modes are located downstream; the spatial contour must be deformed above those originating in the lower half-plane, leading to upstream modes. This is a particularly important point, because this global consideration is the only way to determine rigorously the casual solution, and arguments based on the local group velocity will be seen to be incorrect in a wide variety of cases. This will be considered in detail in § 4.

In summary, it follows that in order to determine the long-time behaviour of our system we need only consider the behaviour of the zeros of the dispersion relation $D(k, \omega) = 0$, and our approach to this problem is described in the next two subsections.

2.3. *Dispersion relation for simple profiles*

The main part of our work is concerned with the behaviour of realistic shear profiles, but initial consideration of simple model profiles, for which analytical dispersion relations can be derived, provides insight into the general problem. The simplest possibility is to consider uniform flow, and thereby set $f(y/\epsilon) \equiv 1$ for all y, as done by Brazier-Smith & Scott (1984) and Crighton & Oswell (1991). They show that the dispersion relation then reduces to a simple quadratic in ω of the form

$$\mathscr{D}_0(k, \omega) \equiv |k|(\omega^2 - k^4) + (Uk - \omega)^2 = 0. \tag{2.8}$$

Note that in general $\mathscr{D}_0(k, \omega)$ will differ from the dispersion function $D(k, \omega)$ appearing in (2.7) by only a multiplicative constant factor, which can be ignored for the purposes of determining the roots of $D(k, \omega) = 0$.

Alternatively, we can consider the broken-line profile corresponding to a region of uniform shear separating the plate from the uniform free-stream, i.e.

$$\begin{aligned} f(y/\epsilon) &= y \quad \text{for} \quad 0 \leqslant y \leqslant \epsilon \\ &= 1 \quad \text{for} \quad y > \epsilon. \end{aligned} \tag{2.9}$$

The Rayleigh equation (2.3) then reduces to Laplace's equation in each of the two

regions, and solving in each separately, applying the boundary condition (2.6) and enforcing continuity of normal velocity and pressure across $y = \epsilon$ we find the dispersion relation to be a cubic in ω of the form

$$\omega^3\epsilon k(1+|k|)\exp(\epsilon|k|)+\omega^2\left[-\epsilon k^2\left(|k|U\exp(\epsilon|k|)-\frac{U}{\epsilon}\sinh(\epsilon|k|)\right)-U|k|\exp(\epsilon|k|)\right.$$
$$\left.+|k|\left(U\cosh(\epsilon|k|)-\epsilon U|k|\exp(\epsilon|k|)\right)\right]$$
$$+\omega\left[U\left(k|k|U\exp(\epsilon|k|)-\frac{kU}{\epsilon}\sinh(\epsilon|k|)\right)-\epsilon k^5|k|\exp(\epsilon|k|)\right]$$
$$+\epsilon k^5\left[k|k|U\exp(\epsilon|k|)-\frac{kU}{\epsilon}\sinh(\epsilon|k|)\right]=0. \tag{2.10}$$

In the limit $\epsilon \to 0$ (i.e. the characteristic length scale of the waves much longer than the boundary-layer thickness), (2.10) reduces exactly to the dispersion relation for uniform flow (2.8) (in fact, the coefficients of $\omega^{1,2,3}$ in (2.10) are $O(\epsilon)$ while the ω^0 term is $O(\epsilon^2)$, so that in this limit we actually obtain the uniform-flow dispersion relation plus the zero root $\omega = 0$).

2.4. *Dispersion relation in the general case*

To investigate the behaviour of more realistic shear profiles, we have chosen to consider the Blasius profile. A property of the Rayleigh equation (2.3) is that its dispersion relation possesses complex conjugate pairs of amplified and damped eigenvalue solutions. However, physically relevant solutions that necessarily match onto viscous solutions at high Reynolds number are obtained by choosing an integration contour that extends from the free-stream boundary to the wall such that the path lies above or below any critical points y_c/ϵ, which are defined by $kUf(y_c/\epsilon) = \omega$, in compliance with Lin's (1955) criterion. For non-neutral eigenvalues $f(y_c/\epsilon)$ is complex and so y_c must be continued into the complex plane. This has been achieved by solving the Blasius similarity equation (where $g'(y/\epsilon) = f(y/\epsilon)$)

$$g''' + gg'' = 0, \tag{2.11}$$

with the boundary conditions given by $g(0) = g'(0) = g'(\infty) - 1 = 0$ and with y and, therefore, g and its derivatives taken to be complex; see Healey (1998), Lingwood (1995) and Olendraru *et al.* (1996).

In practice, (2.11) is integrated along a path given by

$$Y_i = \frac{\sigma Y_r(10 - Y_r)\exp(-Y_r)}{3.329808}, \tag{2.12}$$

where $Y \equiv y/\epsilon$ is the non-dimensional transverse length scale based on the boundary-layer thickness and $Y = Y_r + \mathrm{i}Y_i$, from $Y_r = 0$ to $Y_r = 10$. The numerical denominator was chosen such that the maximum deviation into the complex Y-plane, which occurs at $Y_r \approx 0.900980$, is σ, and the value $Y_r = 10$ was chosen to give a finite free-stream boundary where $f(Y)$ is closely approaching its asymptotic value. This procedure provides complex f and f'' directly for any σ. The Rayleigh equation is then solved numerically for a given set of parameters (ϵ and U) using a shooting algorithm. This procedure starts with the analytical solution in the limit $y \to \infty$, which is given by $\exp(-|k|y)$ ($|k|$ as defined in § 2.1), that satisfies the free-stream boundary condition (i.e. $\bar{\phi}(y;k,\omega) \to 0$ as $y \to \infty$). With only the wall boundary condition (2.6) to be satisfied, either k or ω is specified, while an initial estimate

is made for the other. A double-precision fixed-step-size fourth-order Runge–Kutta integrator and a Newton–Raphson procedure are used to converge onto a value for the initially guessed quantity that satisfies the wall boundary condition to within a predetermined tolerance. In fact, in § 3.2 we will be concerned with saddle points of the dispersion relation in the k-plane, i.e. with eigenvalues for which $\partial\omega/\partial k = 0$. This second condition, together with (2.6), implies that both k and ω must be initially guessed and a two-dimensional Newton–Raphson procedure is needed to converge onto the solution. Nevertheless, the principles are the same.

The precise form of (2.12) is, in fact, unimportant provided it passes on the correct side of Y_c. The magnitude of σ necessary to achieve this is not known *a priori*, but when it is too small spurious solutions are found with Y_c lying on the path of integration. This problem was tested for and the magnitude of σ was increased until the eigenvalue solutions became independent of σ. Note that for certain combinations of parameters there are no critical points. For such cases there is no need to continue y into the complex plane and both eigenvalue solutions that together form a complex conjugate pair are valid.

3. Absolute instability

In this Section we aim to determine the ranges of ϵ–U parameter space over which our system is absolutely unstable. We consider the simple model profiles of § 2.3 first, before moving onto the Blasius profile.

3.1. *Simple model profile*

In the case of uniform flow over the plate, Brazier-Smith & Scott (1984) and Crighton & Oswell (1991) have shown that the system is absolutely unstable for all $U > U_0 \approx 0.074$. The quadratic dispersion relation (2.8) in fact possesses two saddle points in the k-plane, but only one of these is a pinch point. For $U \leqslant U_0$ both saddles lie on the real k-axis with corresponding real ω, but for all $U > U_0$ the pinch saddle moves into the lower half of the k-plane and upper half of the ω-plane, and therefore corresponds to an absolute instability.

The cubic dispersion relation (2.10) for the simple shear profile has three saddle points. Two of these saddle points correspond to the saddles found in the uniform-flow problem, and again just one of them is a genuine pinch. The third saddle does not have a uniform-flow counterpart, but seems to lie at purely real values of k, ω for all U and ϵ, and will therefore not affect the absolute instability. The movement of the pinch point in the k- and ω-planes for varying ϵ at fixed U was investigated by starting from an initial guess for the saddle for small ϵ provided by the uniform-flow result (2.8), and then slowly increasing ϵ and using Newton iteration at each stage to find the genuine saddle of (2.10). This was then repeated for other values of U.

The absolute instability boundaries in ϵ–U space are shown in figure 2. If we consider the behaviour for fixed U as ϵ is increased from zero, then it is clear that there are three quite distinct possibilities. First, if $U > U_0$ then the pinch frequency possesses a strictly positive imaginary part for all ϵ below the value given by the upper boundary in figure 2, leading to absolute instability. Second, for $0.0307 < U < 0.074$ the pinch frequency is strictly real for small ϵ, therefore corresponding to marginal absolute instability (i.e. the system can be at worst convectively unstable, but could potentially become absolutely unstable with the introduction of dissipation, as discussed in a different context in § 5 of Peake 1997). However, the pinch then moves into the upper half of the ω-plane as ϵ is increased across the lower boundary, therefore then

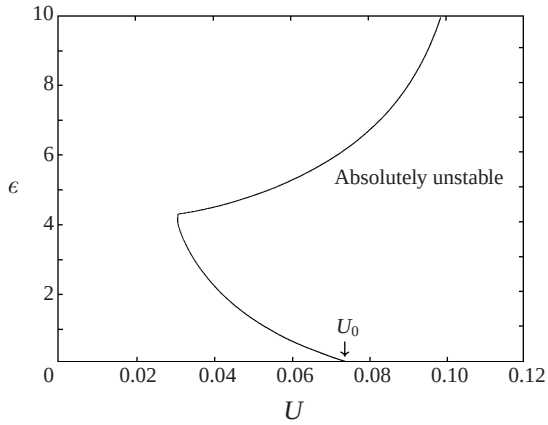

FIGURE 2. The absolute instability boundaries in ϵ–U space for the simple broken-line shear profile.

corresponding to a genuine absolute instability. As ϵ increases still further, then for all $U > 0.0307$ the pinch frequency moves into the lower half of the ω-plane as ϵ crosses the upper boundary in figure 2, and the absolute instability becomes damped so that the system is at worst convectively unstable again. Third, for $U < 0.0307$ the pinch possesses a real frequency for all ϵ, so that the system is only marginally absolutely unstable. The upper and lower absolute instability boundaries merge at $U = 0.0307$, $\epsilon = 4.03$, at which point the pinch point merges with the second (non-pinching) saddle.

It seems that the introduction of simple shear has allowed absolute instability to appear at much lower values of U than in the uniform-flow problem. For definiteness we consider throughout this paper $h_* = 2\,\mathrm{cm}$ steel in water, so that $\rho_* = 1000\,\mathrm{kg\,m^{-3}}$, $m_* = 156\,\mathrm{kg\,m^{-2}}$ and we take the sound speed in the solid, c_*, to be $5300\,\mathrm{m\,s^{-1}}$, leading to $B_*(\equiv m_* h_*^2 c_*^2/12) = 1.46 \times 10^5\,\mathrm{kg\,m^2\,s^{-2}}$. For uniform flow ($\epsilon = 0$) the boundary $U_0(\approx 0.074)$ leads to a minimum dimensional flow speed of $14.5\,\mathrm{m\,s^{-1}}$ for absolute instability, which seems rather larger than might be found in most practical applications. However, for the broken-line profile with $\epsilon > 0$ it seems that absolute instability can occur, at least over some range of ϵ, for any $U > 0.0307$. This leads to a much slower new minimum flow speed for absolute instability of $5.9\,\mathrm{m\,s^{-1}}$, which is a speed which could no doubt be attained in practice. The dimensional boundary-layer thickness for our steel plate is simply $0.15\epsilon\,\mathrm{m}$, so for absolute instability to occur for the lowest possible values of U (for which $\epsilon \approx 4$) we would need the boundary layer to be 0.6 m thick. Of course, for the larger values of U absolute instability is present for much smaller values of ϵ, corresponding to a rather thinner, and perhaps more realistic, boundary layer; e.g. for $U = 0.06$ we need $\epsilon > 0.6$, corresponding to a minimum boundary layer thickness at this speed of 0.09 m.

3.2. *Blasius boundary-layer profile*

We now consider the absolute instability characteristics for a Blasius boundary-layer profile. For this more realistic shear profile, there is no analytical expression for the dispersion relation. Further, $f''(y/\epsilon) \neq 0$ and, therefore, there is a critical layer when $kUf - \omega = 0$. For uniform flow (2.8) shows that the dispersion relation is quadratic, while for the simple broken-line profile (2.10) shows that the dispersion relation has increased to cubic order. For the Blasius profile the number of branches of the dispersion relation increases dramatically.

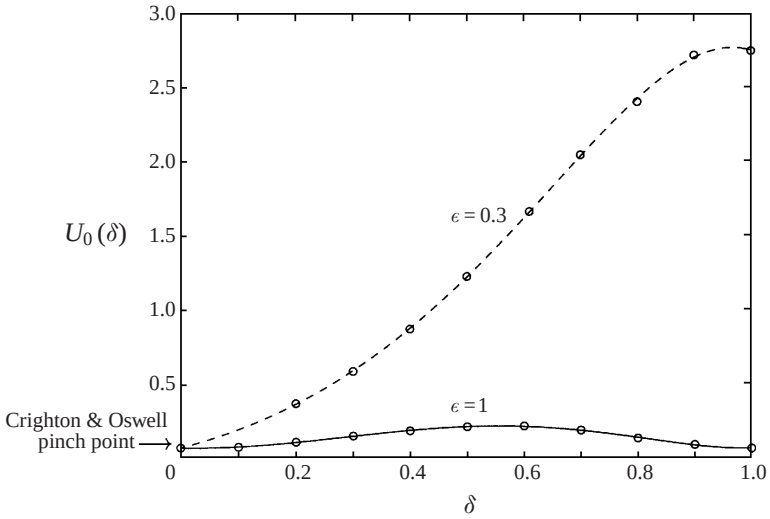

FIGURE 3. $U_0(\delta)$ (where $\mathrm{Im}(\omega) = 0$) for the saddle point corresponding to the Crighton & Oswell saddle point for two values of ϵ.

It is possible to progress smoothly from the Crighton & Oswell result for the onset of absolute instability with a uniform flow, i.e. $U > U_0 \approx 0.074$, to the Blasius-flow case by considering the profile $f(y/\epsilon) = \delta[f_B(y/\epsilon) - 1] + 1$, where here $f_B(y/\epsilon)$ is the Blasius profile. For this model the profile deforms smoothly from uniform flow when $\delta = 0$ to the Blasius profile when $\delta = 1$. Figure 3 shows U_0 as a function of δ for two values of ϵ. When $\delta = 0$, $f'(y/\epsilon) = f''(y/\epsilon) = 0$ and, therefore, the results are independent of ϵ; see (2.3) and (2.6). However, for $\delta = 1$, U_0 differs significantly between $\epsilon = 1$, for which $U_0 \approx 0.061$, and $\epsilon = 0.3$, for which $U_0 \approx 2.74$. Here we have tracked the Crighton & Oswell pinch point from the uniform-flow case to the Blasius-flow case, but this process alone is not sufficient to define the regions of absolute instability for various values of ϵ. The reasons why this process is inconclusive are that there are numerous saddle points of the dispersion relation in the k-plane for Blasius flow, and it is necessary to check whether these are pinching and whether one of these gives rise to absolute instability at a lower value of U than the Crighton & Oswell saddle point; also it is necessary to check that the Crighton & Oswell saddle point remains pinching when $\delta = 1$. Thus $U_0(\delta)$ in figure 3 represents the boundary at which $\mathrm{Im}(\omega)$ of the saddle point corresponding to the Crighton & Oswell saddle point becomes positive, but $U_0(\delta)$ does not necessarily represent the onset of absolute instability.

Figure 4 shows four loci of saddle points of the Blasius-flow dispersion relation in the complex k-plane, i.e. points for which $\partial\omega/\partial k = 0$, for varying U and $\epsilon = 1$. The saddle points on the locus labelled 1 are the Blasius-flow equivalents of the Crighton & Oswell saddle points for varying U (i.e. as shown in figure 3). They are pinching for all U, but $\mathrm{Im}(\omega_0)$ is positive for $\epsilon = 1$ only for $U > U_0 \approx 0.061$, which is marked by the symbol ($\circ$). The saddle points on the loci labelled 2, 3 and 4 are never pinching as well as having $\mathrm{Im}(\omega_0) > 0$, although they do have these properties separately over certain ranges of U. Therefore, for $\epsilon = 1$ none of these other saddle points lead to absolute instability and the flow is only absolutely unstable for $U > U_0 \approx 0.061$.

The uniform-flow and the broken-line flow dispersion relations have no equivalent of the saddle points on the locus labelled 2. This leads to a fundamental difference

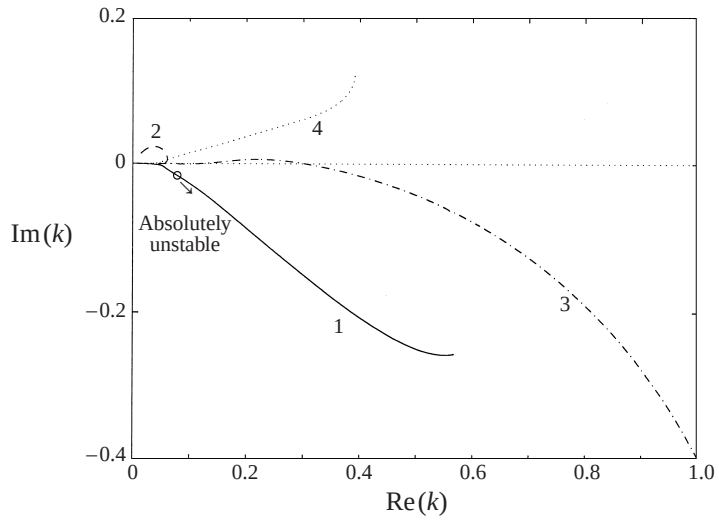

FIGURE 4. Loci of saddle points of the Blasius-flow dispersion relation, $\partial\omega/\partial k = 0$, for varying U and $\epsilon = 1$. U increases along the loci away from the origin.

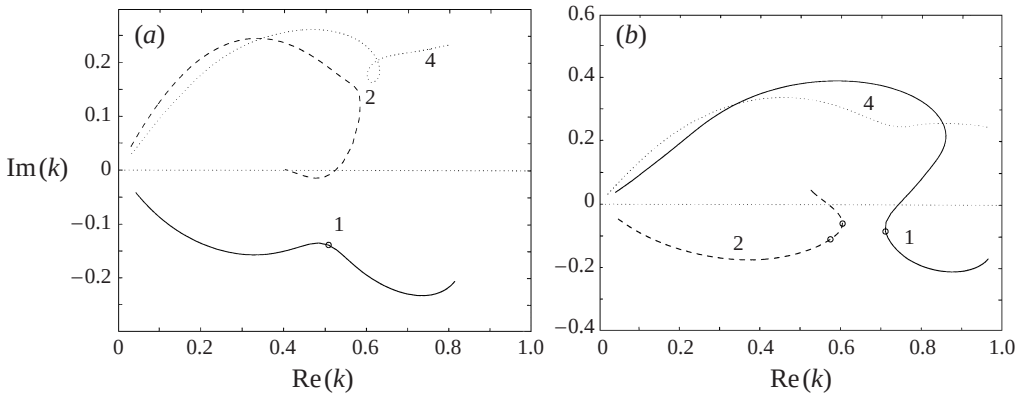

FIGURE 5. Loci of saddle points of the Blasius-flow dispersion relation, $\partial\omega/\partial k = 0$, for varying U and (*a*) $\epsilon = 0.7$ and (*b*) $\epsilon = 0.6$. U increases along the loci away from the origin.

in behaviour as ϵ is reduced to zero, namely in the limit where the boundary-layer thickness becomes negligible compared with the fluid-loading length scale and where one would expect the Blasius results to match onto those for the simple uniform-flow model. Between $\epsilon = 0.7$ and $\epsilon = 0.6$ there is a saddle point of the group-velocity function in the k-plane, i.e. there is a point where $\partial^2\omega/\partial k^2 = 0$ as well as $\partial\omega/\partial k = 0$. At this double saddle point, which occurs between the loci of saddle points labelled 1 and 2, there is branch switching and, therefore, the labelling of the two loci becomes ambiguous. Nevertheless, for $\epsilon \leqslant 0.63$ and as U increases, the pinching saddles are split between loci 1 and 2. Figure 5 shows three loci of saddle points for varying U and $\epsilon = 0.7$ and $\epsilon = 0.6$. The labelling of the loci is consistent with that in figure 4. Figure 6 gives a closer view of the region of the k-plane in which the double saddle point lies and shows the switching between loci 1 and 2.

As ϵ is reduced, this splitting leads to two ranges of U over which the flow is absolutely unstable: see figure 5, where the region of absolute instability on locus

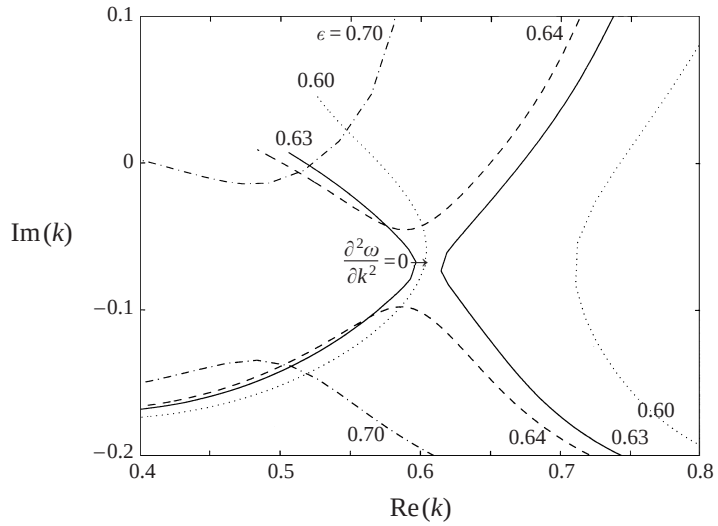

FIGURE 6. Loci 1 and 2 of saddle points of the Blasius-flow dispersion relation for a small range of ϵ between 0.6 and 0.7 and for varying U, showing the double saddle point where $\partial^2\omega/\partial k^2 = 0$.

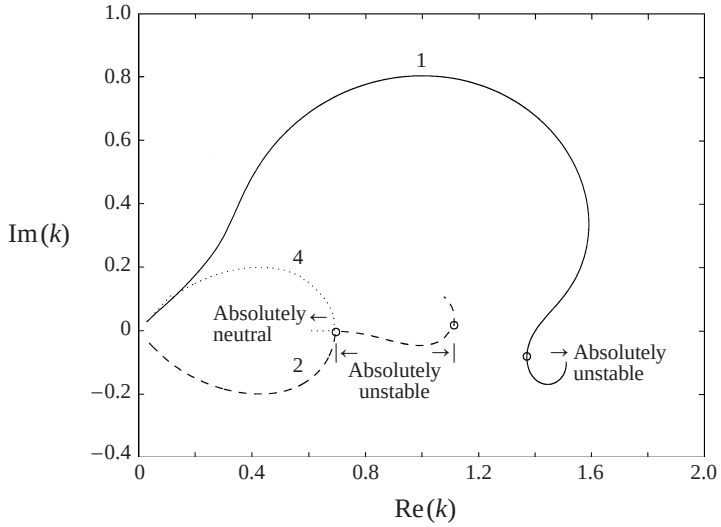

FIGURE 7. Loci of saddle points of the Blasius-flow dispersion relation, $\partial\omega/\partial k = 0$, for varying U and $\epsilon = 0.4$.

1 in both (*a*) and (*b*) lies to the right (higher U) of $\circ$, and on locus 2 in (*b*) the second region lies between the two circles. As ϵ is reduced towards zero, there is a rapid increase in the critical value of U for absolute instability on the locus that we have arbitrarily continued to denote by 1. However, the second bounded (with lower and upper critical values of U) region of absolute instability on locus 2 lies at lower values of U and, therefore, defines the lower limiting value of U for absolute instability; see figure 9. This region on locus 2 expands in range as ϵ is reduced from 0.63. For a value of ϵ around 0.4 there is a further interaction between two of the loci, which results in further splitting of the absolutely unstable range of U; see figure 7. This time the interaction occurs between locus 2 and locus 4. Note that the saddle

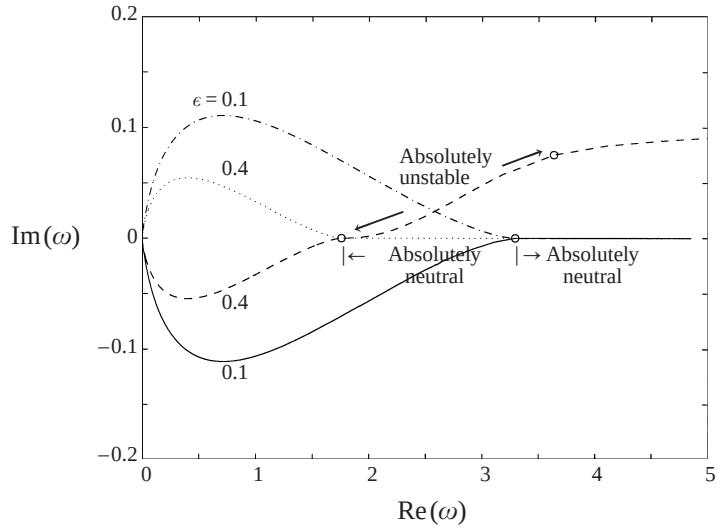

FIGURE 8. Loci 2 and 4 of the Blasius-flow dispersion relation, $\partial\omega/\partial k = 0$, for varying U and $\epsilon = 0.4$ and $\epsilon = 0.1$.

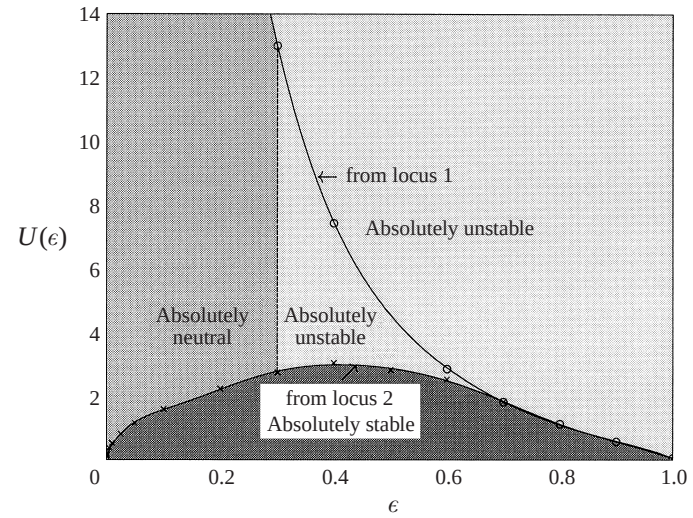

FIGURE 9. Critical values of U for absolute instability and marginal absolute instability as a function of ϵ for the Blasius boundary-layer flow.

points on locus 4 do have equivalent representations in the uniform-flow problem; see Crighton & Oswell's (1991) non-pinching point of zero $\partial\omega/\partial k$. This interaction initially leads to a decrease in the critical value of U for absolute instability with decreasing ϵ. However, with further reduction of ϵ, the pinching saddle points on all but locus 1 never become unstable; at worst they are neutral, i.e. with both k and ω purely real (see figure 9).

Figure 8 compares the behaviour of loci 2 and 4 in the complex ω-plane for $\epsilon = 0.4$ with that for $\epsilon = 0.1$. The critical values of U for these pinching saddle points to change from absolutely stable ($\mathrm{Im}(\omega) < 0$) to absolutely neutral ($\mathrm{Im}(\omega) = 0$) continue to decrease as $\epsilon \to 0$, e.g. for $\epsilon = 0.0005$ the limiting value of U is about

0.12. Numerical difficulties were encountered at values of ϵ closer to zero. Therefore, it is uncertain whether this critical absolutely neutral U approaches zero as $\epsilon \to 0$, or whether it approaches the Crighton & Oswell value of approximately 0.074. In either case, however, it seems to be a relatively uninteresting boundary because it denotes only marginal absolute instability. This feature leaves the onset of absolute instability being determined by the destabilization of the pinching saddles on locus 1. This limit increases monotonically and rapidly with decreasing ϵ. For example, $U_0 \approx 26.8$ at $\epsilon = 0.2$ (out of range in figure 9), which corresponds to a ridiculously high dimensional speed of about $5257\,\mathrm{m\,s^{-1}}$, compared with $U_0 \approx 0.061$ at $\epsilon = 1$, which corresponds to a much more reasonable dimensional speed of about $12\,\mathrm{m\,s^{-1}}$. Figure 9 summarizes the various critical values of U as a function of ϵ.

The results of this subsection show that the topology of the Blasius dispersion relation differs significantly from that of the uniform-flow problem. For this reason, it seems that it is not possible to develop an asymptotic scheme to describe the flow based on the idea of a small departure from the uniform-flow saddle behaviour. The long-wave asymptotic analysis of the present problem, based on the original work by Drazin & Howard (1962), is included in the Appendix for completeness, but the basic result presented there is derived assuming that the Blasius saddle is perturbed, by a small amount $O(\epsilon k)$, from the uniform-flow saddle point. Our numerical results make it clear that this is a good approximation for ϵ larger than about 0.7, but is no longer valid for smaller ϵ, thanks to the collision of the two branches of saddles shown in figure 6.

In summary, the uniform-flow result for absolute instability is a singular limit that the continuously differentiable profile does not approach as $\epsilon \to 0$. One difference between the uniform-flow case and the Blasius case is that the latter has a zero steady-slip condition, which means that the normal-velocity boundary condition is $\partial\eta/\partial t = -\partial\phi/\partial x$ for $\epsilon \neq 0$ in our problem, while in the uniform-flow problem ($\epsilon = 0$) it is $\partial\eta/\partial t + U\partial\eta/\partial x = -\partial\phi/\partial x$. However, unlike the uniform-flow problem, the broken-line profile does correctly model the steady streamwise velocity on the wall and yet the broken-line result matches onto the uniform-flow result in the limit $\epsilon \to 0$, and it therefore seems likely that the introduction of the critical layer is the fundamental factor that distinguishes the physical (smooth) shear-layer profiles from the simplistic model ones. Nevertheless, for sufficiently large ϵ, the critical speed for the onset of absolute instability becomes increasingly physically realizable.

4. Anomalous modes

4.1. *Simple model profile*

Neutral anomalous modes were first identified for the uniform-flow problem by Brazier-Smith & Scott (1984), and analysed in detail by Crighton & Oswell (1991). They correspond to neutral waves located downstream of the driver but with group velocity pointing towards the driver, in contradiction of the usual radiation condition of out-going energy propagation at infinity. For the simple broken-line profile described in § 2.3, neutral anomalous modes can also be identified, and indeed the results are qualitatively similar to those found for uniform flow. Essentially, the dispersion curve for our broken-line profile looks very much like the curves plotted by Crighton & Oswell (see for example their figure 6). Just as in the uniform-flow case, we find that an anomalous neutral mode exists over a restricted frequency range, bounded above by a point at which the group velocity is infinite ($k = k_b$ in Crighton & Oswell's

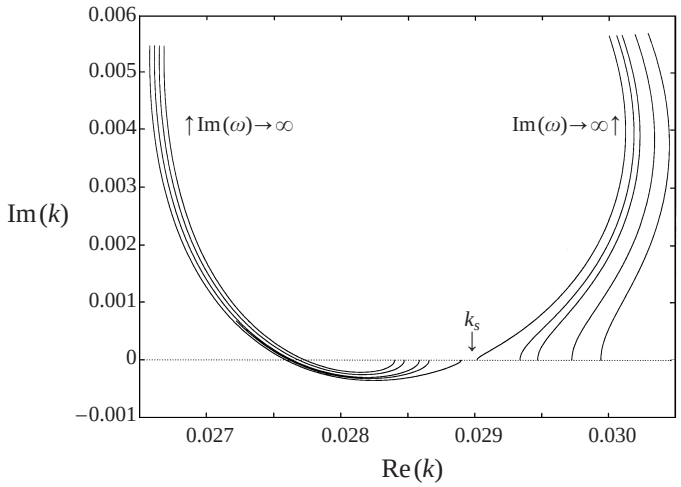

FIGURE 10. Motion of modes in the k-plane as $\mathrm{Im}\,(\omega)$ is increased from zero and with $\mathrm{Re}\,(\omega)$ kept constant. Here we have results for the simple broken-line profile of § 2.3, with $\epsilon = 0.5$, $U = 0.025$. The group velocity vanishes at $k_s = 0.02896$.

notation) and bounded below by a point where it is zero ($k = k_s$). In figure 10 we show the behaviour of various modes close to $k = k_s$ as $\mathrm{Im}\,(\omega)$ is increased from zero. The anomalous behaviour for the modes with $k < k_s$ can clearly be seen; these modes originate from the upper half-plane for large $\mathrm{Im}\,(\omega)$, indicating that they are located downstream of the driver, but their local group velocity is negative, and is therefore directed towards the driver. The modes with $k > k_s$ behave conventionally. A full parametric study of the occurrence of these modes for our broken-line profile does not seem necessary, and we merely note here that they are apparently present for all values of ϵ and U for which the flow is not absolutely unstable.

4.2. *Blasius boundary-layer profile*

Figure 11 shows the temporal ($\mathrm{Im}\,(k) = 0$) dispersion curve for $\epsilon = 1$ and $U = 0.05$ for the Blasius boundary-layer flow; both $\mathrm{Re}\,(\omega)$ and $\mathrm{Im}\,(\omega)$ are given. This figure is based on Crighton & Oswell's (1991) figure 6 for neutral waves in the uniform-flow model. In figure 11 the dashed-dotted line represents $\mathrm{Re}\,(\omega) = Uk$. For eigenvalues with $\mathrm{Re}\,(\omega)$ above this line, the phase speed of the disturbance wave is greater than the free-stream speed and, therefore, there is no critical layer. Here the dispersion relation is real, namely $\mathrm{Im}\,(\omega) = \mathrm{Im}\,(k) = 0$. However, when $\mathrm{Re}\,(\omega) < Uk$ there will be a critical layer somewhere within the boundary layer and, in general, the dispersion relation is now complex. Nevertheless, by keeping k real, we form a temporal dispersion curve that is not dissimilar to Crighton & Oswell's (1991) neutral dispersion curve (their figure 6). In particular, we have a branch point in the k-plane, i.e. a point where $\partial k/\partial\omega = 0$, close to the real k-axis near to $\mathrm{Re}\,(k) = 0.06$, which corresponds to the Crighton & Oswell neutral branch point denoted by (k_b, ω_b) that marks the upper wavenumber limit for temporal instability in their uniform-flow model.

The Crighton & Oswell dispersion relation also has two real saddle points close to this branch point; see the turning points on the lower branch of their figure 6. They denote these two saddle points by (k_s, ω_s) and (k_p, ω_p), where only the latter is a pinching saddle. We also have two saddle points close to our branch point and a third at higher k, which is not shown in figure 11 but is close to a minimum in $\mathrm{Re}\,(\omega)$

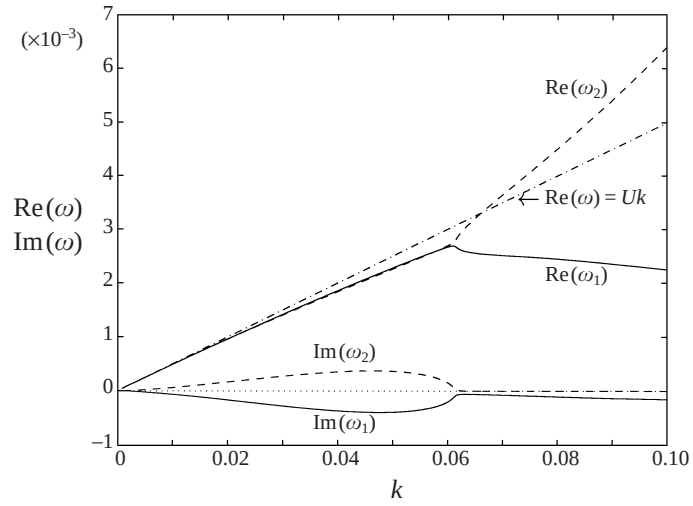

FIGURE 11. Temporal dispersion curve for $\epsilon = 1$ and $U = 0.05$ for the Blasius boundary-layer flow ($\mathrm{Im}\,(k) = 0$).

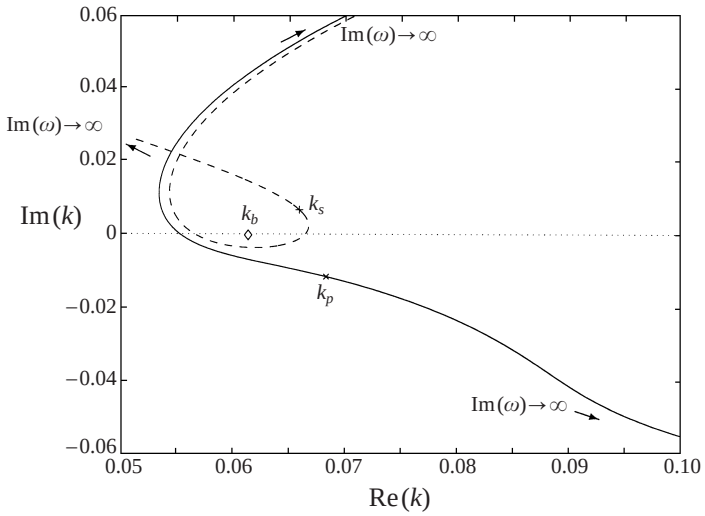

FIGURE 12. Loci of $k(\omega)$ as $\mathrm{Im}\,(\omega) \to \infty$ and $\mathrm{Re}\,(\omega)$ fixed at the saddle-point values for $\epsilon = 1$ and $U = 0.05$ for the Blasius boundary-layer flow. The branch point, $\partial k/\partial\omega = 0$, is also shown.

at $k \approx 0.123$ in figure 14 (which shows simply $\mathrm{Re}\,(\omega_1)$ and $\mathrm{Im}\,(\omega_1)$ as in figure 11, but plotted over a larger range), but these saddle points do not lie exactly on the real k-axis. Furthermore, as discussed earlier in the context of absolute instability for the Blasius boundary-layer flow, there are numerous other saddle points of the dispersion relation for a given ϵ and U elsewhere in the complex k-plane. Here, we shall restrict our attention to these three that lie close to the real k-axis.

Figure 12 shows the relative positions of the branch point and the neighbouring two saddle points in the complex k-plane with the loci of $k(\omega)$ as $\mathrm{Im}\,(\omega) \to \infty$ with $\mathrm{Re}\,(\omega)$ constant. Following the notation of Crighton & Oswell, the saddle point in the lower half-k-plane is pinching and is therefore (k_p, ω_p); the saddle point in the upper half-k-plane is non-pinching and is therefore (k_s, ω_s). The branch point is denoted by

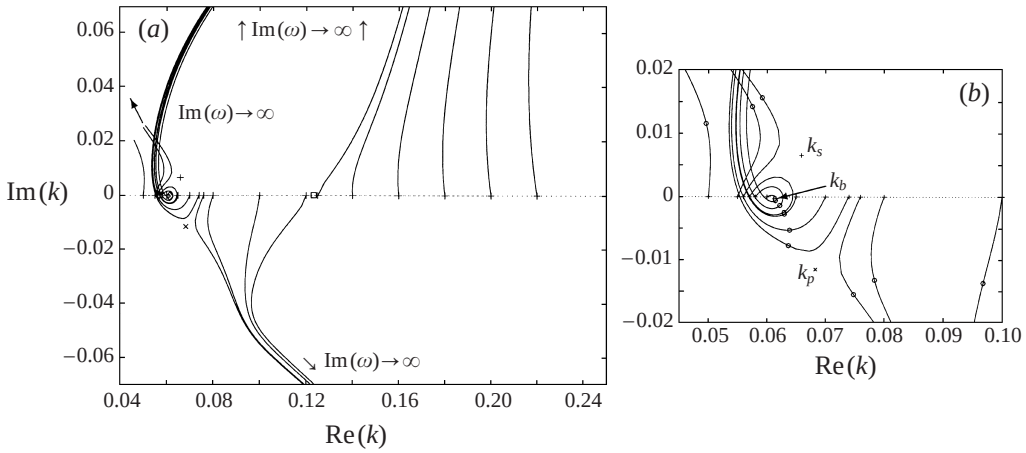

FIGURE 13. (*a*) Loci of $k(\omega)$ as $\mathrm{Im}\,(\omega) \to \infty$ and $\mathrm{Re}\,(\omega)$ fixed for $\epsilon = 1$ and $U = 0.05$ for the Blasius boundary-layer flow. (*b*) A magnified view. The circles ($\circ$) in (*b*) indicate the points on the loci where $\mathrm{Im}\,(\omega) = 0$. The saddle points and branch point are also shown.

(k_b, ω_b). Note that these two saddle points lie on loci 1 and 4, respectively, in figure 4. The pinch point occurs between a spatially damped upstream-propagating mode and a spatially growing downstream-propagating mode. The non-pinching saddle point is a coalescence of two downstream modes that are spatially damped at the saddle point itself. One of these coalescing downstream modes is showing behaviour reminiscent of the anomalous propagation behaviour described by Crighton & Oswell (1991) for their neutral uniform-flow modes.

For the Blasius boundary-layer flow the dispersion relation is, in general, complex rather than real and, therefore, the anomalous propagation occurs for non-neutral rather than neutral modes. This fact complicates the situation because now the group velocity is also complex and physical interpretation of its meaning is unclear. Often, in such cases, the real part of the complex quantity $\partial\omega/\partial k$ is used to define the group velocity, while the imaginary part is ignored. This approximation is not justifiable and, further, $\mathrm{Re}\,(\partial\omega/\partial k)$ can change sign in the same way as the purely real group velocity for the anomalously propagating neutral mode in the uniform-flow model. This behaviour is shown by the loci of increasing $\mathrm{Im}\,(\omega)$ in figure 12 by the coalescing downstream mode that approaches k_s from below. (By the Cauchy–Riemann relations, $\mathrm{Re}\,(\partial\omega/\partial k) = \partial\mathrm{Re}\,(\omega)/\partial\mathrm{Re}\,(k) = \partial\mathrm{Im}\,(\omega)/\partial\mathrm{Im}\,(k)$ and, therefore the change in $\mathrm{Im}\,(k)$ with increasing $\mathrm{Im}\,(\omega)$ on the loci in this figure indicates the sign of $\mathrm{Re}\,(\partial\omega/\partial k)$.) The proximity of the branch point to the non-pinching saddle point is not unexpected; see Lingwood (1997).

Figure 13 summarizes the propagation behaviour for modes on the branch marked with the solid line (ω_1) in figure 11 over a range of $\mathrm{Re}\,(k)$ for $\epsilon = 1$ and $U = 0.05$, which is a value of U below the threshold of absolute instability for this value of ϵ. Figure 14 gives ω_1 again, but over a larger range of $\mathrm{Re}\,(k)$ than figure 11, and summarizes the divisions between different propagation behaviour. For sufficiently small and sufficiently large $\mathrm{Re}\,(k)$ (i.e. $\mathrm{Re}\,(k) < 0.057$ and $\mathrm{Re}\,(k) > 0.123$) the propagation behaviour is straightforward. The the local sign of $\mathrm{Re}\,(\partial\omega/\partial k)$ is positive and globally the mode originates in the upper half-k-plane for large positive $\mathrm{Im}\,(\omega)$. Thus the mode exists in the region downstream of the driver and radiates outwards from the driver. A similarly straightforward behaviour exists for $0.075 < \mathrm{Re}\,(k) < 0.123$, where the

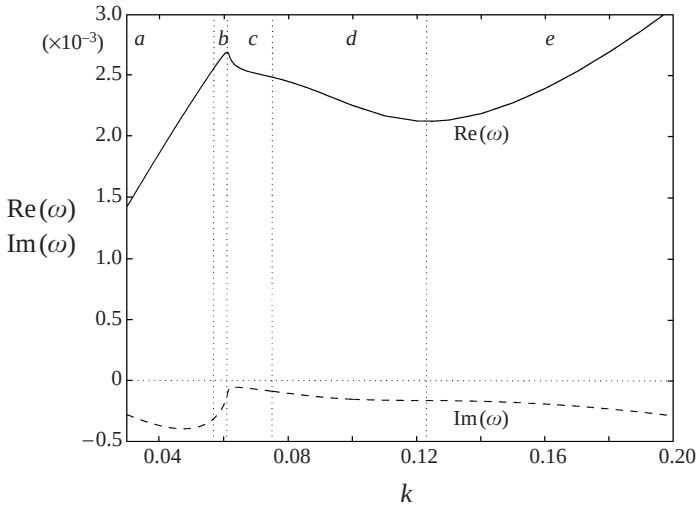

FIGURE 14. Part of the temporal dispersion relation for $\epsilon = 1$ and $U = 0.05$, i.e. ω_1 of figure 11. The labels *a*, *b*, *c*, *d*, *e* represent, respectively, standard-downstream, doubly anomalous, singly anomalous, standard-upstream and standard-downstream propagation behaviour.

local sign of $\mathrm{Re}(\partial\omega/\partial k)$ is negative and globally the mode originates in the lower half-k-plane for large positive $\mathrm{Im}(\omega)$. So over this range of $\mathrm{Re}(k)$ the mode radiates outward from the driver in the upstream direction.

For $0.061 < \mathrm{Re}(k) < 0.075$ there is singly-anomalous behaviour, i.e. locally the sign of $\mathrm{Re}(\partial\omega/\partial k)$ is negative but globally the mode originates in the upper half-k-plane for large positive $\mathrm{Im}(\omega)$. Further, for $0.057 < \mathrm{Re}(k) < 0.061$, there is doubly anomalous behaviour, where the local sign of $\mathrm{Re}(\partial\omega/\partial k)$ is positive and globally the mode originates in the upper half-k-plane for large positive $\mathrm{Im}(\omega)$, but the loci reverse direction twice before ending up in the upper half-k-plane. As mentioned earlier these modes are non-neutral, therefore perhaps the most relevant points on the loci to consider are those where $\mathrm{Im}(\omega) = 0$ (marked by $\circ$ in figure 13). These points represent the spatial eigenvalues that would be calculated from given real ω with the sign of $\mathrm{Im}(k)$ denoting spatial growth or decay.

Without the results of the Briggs–Bers analysis shown in figure 13 there would be doubt about the region of existence of these spatial modes and whether they are growing or decaying. For example, in the singly anomalous region and while the point of $\mathrm{Im}(\omega) = 0$ is to the right of the minimum turning point in the loci of $k(\omega)$ as $\mathrm{Im}(\omega) \to \infty$, a naive consideration of the propagation characteristics of these spatial modes would suggest that they are stable outwardly radiating upstream modes, whereas in reality the Briggs–Bers technique has shown that they are inwardly radiating downstream modes. The same is true of the points of $\mathrm{Im}(\omega) = 0$ in the doubly anomalous region, which all lie to the right of the minimum in the loci; namely their spatial location and propagation characteristics cannot be predicted from their local group velocities. Note that the propagation behaviour of the modes on the dashed branch (ω_2) of figure 11 is never anomalous; these modes are outward-radiating downstream modes for all $\mathrm{Re}(k)$.

It is clear from figure 13 that the topology of the dispersion relation is determined by the saddle points and branch point, which therefore play a fundamental role in determining the boundaries between the different propagation characteristics. A local

analysis of the dispersion relation predicts the change in k with small changes in $\mathrm{Im}\,(\omega)$ denoted by δ ($\delta > 0$). That is, the Taylor expansion for $k(\omega + \mathrm{i}\delta)$ shows that

$$\Delta[\mathrm{Re}\,(k)] = -\delta \mathrm{Im}\left(\frac{\partial k}{\partial \omega}\right) - \frac{\delta^2}{2}\mathrm{Re}\left(\frac{\partial^2 k}{\partial \omega^2}\right) + \frac{\delta^3}{6}\mathrm{Im}\left(\frac{\partial^3 k}{\partial \omega^3}\right) + \cdots, \tag{4.1}$$

$$\Delta[\mathrm{Im}\,(k)] = \delta \mathrm{Re}\left(\frac{\partial k}{\partial \omega}\right) - \frac{\delta^2}{2}\mathrm{Im}\left(\frac{\partial^2 k}{\partial \omega^2}\right) - \frac{\delta^3}{6}\mathrm{Re}\left(\frac{\partial^3 k}{\partial \omega^3}\right) + \cdots . \tag{4.2}$$

If we consider the boundaries between different propagation characteristics in figure 14 then at $k \approx 0.057$ the behaviour changes from standard-downstream to doubly anomalous. This is characterized by a point where $\mathrm{Im}\,(\partial^2 k/\partial \omega^2) = 0$ (going from negative to positive with increasing $\mathrm{Re}\,(k)$). This can be predicted by (4.2) because the difference in behaviour is characterized by $\mathrm{Im}\,(k)$ as $\mathrm{Im}\,(\omega) \to \infty$ (with constant $\mathrm{Re}\,(\omega)$) changing from increasing monotonically to increasing and then turning around twice. In the first and second cases, respectively, the three terms in (4.2) must have the following signs:

$$\mathrm{Re}\left(\frac{\partial k}{\partial \omega}\right) > 0, \quad \mathrm{Im}\left(\frac{\partial^2 k}{\partial \omega^2}\right) < 0, \quad \mathrm{Re}\left(\frac{\partial^3 k}{\partial \omega^3}\right) < 0, \tag{4.3}$$

$$\mathrm{Re}\left(\frac{\partial k}{\partial \omega}\right) > 0, \quad \mathrm{Im}\left(\frac{\partial^2 k}{\partial \omega^2}\right) > 0, \quad \mathrm{Re}\left(\frac{\partial^3 k}{\partial \omega^3}\right) < 0. \tag{4.4}$$

Thus, the change in propagation behaviour is characterized by a change in sign of the imaginary part of the second derivative. Similar considerations show that the change from doubly to singly anomalous behaviour occurs when $\mathrm{Re}\,(\partial k/\partial \omega)$ changes from positive to negative at $k \approx 0.061$. This change of sign implies that $\mathrm{Im}\,(k)$ decreases and then turns around once to increase, rather than increasing first and then turning around twice before continuing to increase. The change from singly anomalous to standard-upstream behaviour at $k \approx 0.075$ (i.e. to monotonic decrease in $\mathrm{Im}\,(k)$) is due to a change in sign of $\mathrm{Im}\,(\partial^2 \omega/\partial k^2)$ (negative to positive with increasing $\mathrm{Re}\,(k)$). The final change between standard-upstream and standard-downstream propagation at $k \approx 0.123$ is marked by $\mathrm{Im}\,(\partial^2 \omega/\partial k^2)$ becoming negative again. The last two changes in behaviour at $k \approx 0.075$ and at $k \approx 0.123$ are not predicted by (4.2), instead they are determined by the presence of the two saddle points ($\partial \omega/\partial k = 0$) close to these values of k. By definition, there are two regions of 'high-ground' in an area of a complex plane containing a saddle point. In this case, there must be two areas of increasing $\mathrm{Im}\,(\omega(k))$ surrounding a point of $\partial \omega/\partial k = 0$ in the complex k-plane. As $\mathrm{Re}\,(k)$ increases above $k \approx 0.075$ in figure 13, the loci switch from passing through the area of high-ground on one side of the saddle point to that on the other side, and a local analysis of the dispersion relation in the vicinity of the saddle point shows that this switching is characterized by a change in sign of $\mathrm{Im}\,(\partial^2 \omega/\partial k^2)$.

5. Start-up problem for uniform flow

In the previous Section we demonstrated how, in the limit $t \to \infty$, the Briggs–Bers technique predicts the existence of modes with anomalous-propagation properties in our shear-layer problem, in much the same way as found by Crighton & Oswell (1991) for uniform flow. One criticism of this conclusion, however, is that the limit $t \to \infty$ could be singular, in the sense that at any large, but finite, time all the waves might behave conventionally. In order to investigate this point we therefore attempt

to analyse the finite-time response to single-frequency forcing (frequency ω_0, say) that is turned on at $t = 0$.

For definiteness and simplicity we restrict attention here to the problem of uniform mean flow, although the same approach could clearly be applied to our shear flow as well (but with greater complexity, given that the dispersion relation is then not available in closed form). In fact, we are simply going to extend the calculations of Brazier-Smith & Scott (1984), who investigated the response to impulsive forcing. For arbitrary forcing switched on at $t = 0$, the plate displacement can be written down in the form given in (2.7), and if we suppose that the flow speed is sufficiently low for the system to be absolutely stable, then the ω-contour can be deformed down onto the real axis to give a double integral in the form

$$\eta(x,t) = \frac{1}{4\pi^2}\int_{-\infty}^{\infty} \exp(-\mathrm{i}\omega t)\overline{F}_0(\omega)\Psi(x,\omega)\mathrm{d}\omega, \tag{5.1}$$

where

$$\Psi(x,\omega) = \int_{L(\omega)} \frac{|k|\exp(\mathrm{i}kx)}{\mathscr{D}_0(k,\omega)}\mathrm{d}k, \tag{5.2}$$

the contour $L(\omega)$ is the real k-axis that has been deformed below or above singularities according to the procedure described in § 2.2, and we recall that $\overline{F}_0(\omega)$ is the transform of the forcing $F(t)$. These integrals cannot be completed in closed form, but their numerical evaluation proceeds in a relatively straightforward manner. First of all, $\Psi(k,\omega)$ is evaluated using exactly the method described in detail by Brazier-Smith & Scott (1984), and only the briefest outline need be given here. Essentially, positive and negative k are considered separately, the respective integrands are resolved into partial fractions, and the resulting integrals converted into standard exponential integrals by deformation of the contours, with suitable pole contributions from the zeros of $\mathscr{D}_0(k,\omega)$ depending on their position relative to $L(\omega)$ and on the sign of x.

Turning to the outer ω-integral, we consider only real forcing functions $F(t)$, and the Hermitian conjugacy of the integrand in (5.1) leads to the fact that only the range $\omega \geqslant 0$ needs to be computed. Two numerical difficulties are a logarithmic singularity at $\omega = 0$, which is subtracted from $\Psi(x,\omega)$ before the ω-integration is completed, and an inverse square-root singularity at $\omega = \omega_p$, which is removed by splitting the integration at $\omega = \omega_p$ and then applying suitable transformations to each portion separately. Full details of this are given in Brazier-Smith & Scott (1984), but an additional feature here is that our forcing transform $\overline{F}_0(\omega)$ will possess a pole on the real axis at $\omega = \omega_0$. In order to guarantee that our solution is zero for $t < 0$, we must therefore deform the ω-contour in (5.1) above this pole; the resulting integral then includes a contribution of $-\pi\mathrm{i}$ times the residue at $\omega = \omega_0$, plus the contribution from the integral on the real axis, which can be handled numerically using a standard Cauchy principal-value routine. All the integrals are now amenable to numerical evaluation using standard routines, and we need only note here that the infinite portion of the ω-integral (i.e. $\omega > \omega_p$) can be evaluated efficiently using Shanks transforms.

We consider two different forcing functions. First, we have single-frequency forcing turned on at $t = 0$ with constant amplitude, i.e.

$$f(t) = \sin(\omega_0 t)\mathrm{H}(t), \tag{5.3}$$

with $\mathrm{H}(t)$ being the unit step function, and the evolution of the plate deflection is shown in figure 15. Here ω_0 is chosen to lie within Crighton & Oswell's (1991) anoma-

lous neutral range, and they then predict that in the limit $t \to \infty$ two neutral waves will be found upstream (both conventional) and two downstream (one conventional, the other anomalous) of the driver. Since the start-up signal must certainly contain frequency components which lie in Crighton & Oswell's convectively unstable regime, it follows that we first see (in figure 15*a*, *b*) a convectively growing head wave that propagates to the right, and which, by the time it has reached the extreme right-hand side of the figure, has grown to large amplitude. Note that the real part of the group velocity of the convectively unstable waves is $O(U)$, and the numerically small size of U explains why relatively large values of t are required before the head wave has propagated out of the figures. Behind the head wave, wave patterns are seen to form upstream and downstream of the driver, and by $t = 1.35 \times 10^5$ these patterns have developed a steady-state form that is very similar to the deflection predicted from the Briggs–Bers theory. (The Briggs–Bers prediction can be simply recovered from the numerical procedure described above by retaining just the contributions from the temporal pole $\omega = \omega_0$ and the corresponding k-poles.)

In figure 15(*c*), the wave pattern downstream of the driver clearly arises from the interference between two waves, and together with the good agreement with the Briggs–Bers prediction shown in figure 15(*d*) this confirms that the anomalous wave is indeed found downstream at a finite value of t. For this value of ω_0, the two downstream modes have wavenumbers of approximately 0.049 and 0.058, leading to an interference pattern with approximate wavelength 120 and modulation length 1400, as can be seen in figure 15(*c*, *d*). The interference pattern downstream can only extend over a finite distance at any given t, depending on the position of the convecting transients, but of course this distance will increase with t. We note that upstream of the driver two (conventional) modes are also present; for larger values of t than shown in figure 15(*c*), the amplitude of one of these modes will increase towards the amplitude of the other one, leading eventually to an interference pattern which is rather closer to that seen in figure 15(*d*).

Second, we suppose that the forcing amplitude is built up more gradually from $t = 0$, with growth rate δ ($\delta \ll \omega_0$) for $t \leqslant T$, before maintaining constant amplitude for $t > T$, i.e.

$$\begin{aligned} f(t) &= \exp(\delta(t - T))\sin(\omega_0 t)\mathrm{H}(t) \quad \text{for} \quad t \leqslant T \\ &= \sin(\omega_0 t) \quad \text{for} \quad t > T. \end{aligned} \tag{5.4}$$

This history is intended to mimic the Rayleigh–Lighthill model of slow amplitude growth, and in order to achieve this we will need to choose T to be very large, so that the system has time to reach an equilibrium state before the forcing switches to constant amplitude. Of course, the Rayleigh–Lighthill model is based on slow amplitude growth from $t = -\infty$, but clearly this cannot be represented within our initial-value formulation. Even so, we believe that studying the forcing (5.4) here is useful, since a naive numerical implementation of the Rayleigh–Lighthill procedure might well be completed in this way. In figure 16 we can see that the response at time $t = T$ appears to be very similar to what would be expected from the Briggs–Bers solution (cf. figure 15*d*), and in particular that again two neutral waves are present downstream of the driver. Calculations for $t > T$ (i.e. once the driver amplitude has become constant) show that the system response continues to be correctly predicted by the Briggs–Bers solution, as in figure 15. As noted previously, the Rayleigh–Lighthill criterion implies that there should only be one neutral wave downstream of the driver. Crighton & Oswell (1991) have already pointed out that

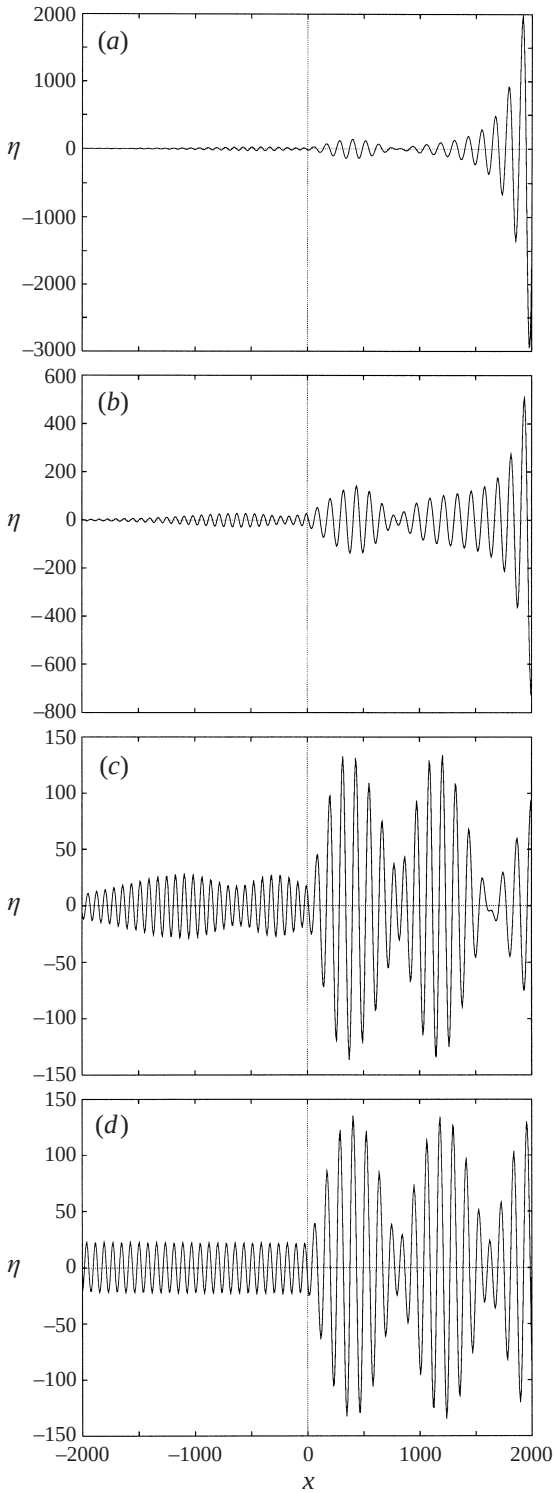

FIGURE 15. Evolution of plate deflection with time. The driver is located at $x = 0$; and $\omega = 0.0023$, $U = 0.05$. (*a*) $t = 1 \times 10^5$, (*b*) 1.2×10^5, (*c*) 1.35×10^5; (*d*) the $t \to \infty$ solution evaluated at $t = 1.35 \times 10^5$. Note the different vertical scales.

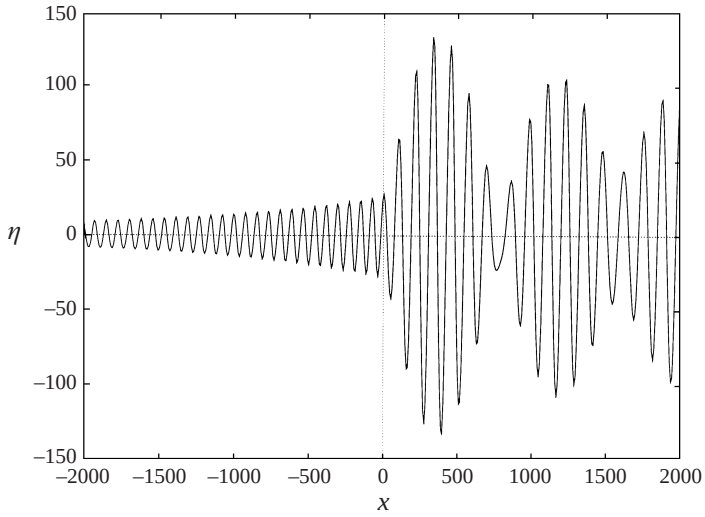

FIGURE 16. Evolution of plate deflection with time, now with slow build up of amplitude: $\omega = 0.0023$, $U = 0.05$, $\delta = 10^{-5}$, $T = 10^6$ and $t = 10^6$.

the Rayleigh–Lighthill criterion was formulated for problems in which the driver is the only source of wave energy, and that in the present problem the mean flow can act as an additional energy source, leading to the possibility of energy being transferred from the flow into the plate through the driver. The results presented in this section confirm that radiation conditions based on the evaluation of modal local group velocity must be used with caution. What is needed in any given problem are the sort of global considerations of the dispersion function advocated by Briggs (1964) and Bers (1983).

6. Conclusions

We have considered the causal response of an inviscid shear-layer flow over an infinite elastic surface subjected to time-harmonic line forcing. Brazier-Smith & Scott (1984) and Crighton & Oswell (1991) have analysed the long-time limit of the response for the case of uniform flow, for which they found absolutely instability for sufficiently high flow speeds and anomalous-propagating neutral modes at lower speeds. Here we have considered more realistic boundary-layer flows.

For a simple broken-line shear profile, for which there is an analytical description of the dispersion relation, we find that the absolute-instability results are qualitatively similar to those for uniform flow. The uniform-flow results are recovered as $\epsilon \to 0$ (the limit in which the shear-layer thickness becomes small), while the introduction of shear allows absolute instability over a range of ϵ at lower, and therefore more easily attainable, values of U than for the uniform-flow problem. However, the more realistic Blasius profile gives results significantly different from the uniform-flow and broken-line cases. This difference is essentially due to the presence of the critical layer, but the fact that the normal-velocity boundary condition in our shear-layer problem does not contain the convective derivative of the plate deflection (see the end of § 3) may also be a contributing factor. In particular, we have found saddle points that are not represented in either the uniform-flow or the broken-line cases, and that as $\epsilon \to 0$

the minimum flow speed required for absolute instability is considerably higher than was found for uniform flow.

In contrast, we find that the uniform-flow anomalous modes do persist for non-zero shear over a wide range of ϵ, although they are non-neutral for the Blasius dispersion relation. Unlike the uniform-flow case, the k-loci of the Blasius-flow modes may change direction more than once as the imaginary part of ω is increased, and we describe this behaviour as 'doubly anomalous' to distinguish it from the (singly) anomalous behaviour that also exists and is familar from the uniform-flow case and a number of other fluid systems. Thus, in general, consideration of the local group velocity cannot accurately predict the spatial location and propagation of the modes. Changes in this propagation behaviour have been related to properties of the dispersion relation. Furthermore, we have found that, after initial transients have convected away, the anomalous mode is present at finite times for both for impulsive start-up and for the forcing that slowly increases to a saturated amplitude. We therefore conclude that the presence of anomalous modes is not a singular feature introduced by taking the long-time limit in the Briggs–Bers procedure. The existence of such anomalous modes, even at $O(1)$ times, means that radiation conditions of out-going group velocity cannot be applied.

R. J. L. acknowledges the support provided by a Research Fellowship at Pembroke College, Cambridge, and a Dorothy Hodgkin Royal Society Fellowship. The authors note that Professor I. D. Abrahams has been undertaking similar work.

Appendix

In this Appendix we describe for completeness asymptotic analysis of absolute instability in the limit of small $k\epsilon$, corresponding to the regime in which the wavelength is much longer than the boundary-layer thickness. We use the long-wave analysis of Drazin & Howard (1962), who determined the long-wave instability properties of unbounded free shear layers, the difference here being that we apply the elastic-wall boundary condition (2.6). The starting point is to define again the transverse coordinate $Y \equiv y/\epsilon$ scaled on the boundary-layer thickness, and then as in Drazin & Howard (1962) introduce the expansion

$$\overline{\phi}(Y;k,\omega) = \exp(-|k|Y)\sum_{n=0}^{\infty}(k\epsilon)^n\chi_n(Y;k,\omega), \tag{A 1}$$

which is then substituted into (2.3). By equating powers of $k\epsilon$ and applying the condition of zero disturbance far from the wall, the first three terms can be determined exactly as in Drazin & Howard (1962), and these are included here for completeness as

$$\left.\begin{aligned}
\chi_0(Y;k,\omega) &= W(Y;k,\omega),\\
\chi_1(Y;k,\omega) &= -\chi_0(Y;k,\omega)\int_Y^{\infty}\left[1-\left(\frac{W(\infty;k,\omega)}{W(Y';k,\omega)}\right)^2\right]\mathrm{d}Y',\\
\chi_2(Y;k,\omega) &= 2W(Y;k,\omega)\int_Y^{\infty}\frac{\mathrm{d}Y'}{W(Y';k,\omega)^2}\int_{Y'}^{\infty}\mathrm{d}Y''W(Y'';k,\omega)\chi_1'(Y'';k,\omega),
\end{aligned}\right\} \tag{A 2}$$

where $W(Y;k,\omega) \equiv kUf(Y) - \omega$. It should be noted that the integrals in (A 2) are only well-defined provided that the flow does not possess a real critical layer (so that $W(Y;k,\omega) \neq 0$ for real Y). We now substitute (A 2) into the boundary condition (2.6) and retain terms up to and including $O(k\epsilon)^2$, to find the modified dispersion relation in the form

$$\mathscr{D}_0(k,\omega) = k\epsilon F(k,\omega), \tag{A 3}$$

where

$$F(k,\omega) = \int_0^\infty \left[1 - \left(\frac{W(\infty;k,\omega)}{W(Y;k,\omega)}\right)^2\right] \left\{W^2(\infty;k,\omega) + W^2(Y;k,\omega)\right\} \mathrm{d}Y \tag{A 4}$$

and we recall that $\mathscr{D}_0(k,\omega)$ is defined in (2.8) and corresponds to the dispersion relation for uniform flow.

Our approach now is to assume that there is a saddle point of the new dispersion relation close to the uniform-flow saddle, at the point $k = k_0 + k_0\epsilon k_1 + \cdots$, $\omega = \omega_0 + k_0\epsilon\omega_1 + \cdots$, where k_0, ω_0 is the saddle point corresponding to absolute instability in uniform flow (so that both $\mathscr{D}_0$ and its first k derivative vanish at $k = k_0$, $\omega = \omega_0$). It is a straightforward matter to show that

$$\omega_1 = \frac{F(k,\omega_0)}{\partial\mathscr{D}_0(k,\omega_0)/\partial\omega}, \quad k_1 = \left[\frac{\dfrac{F}{k} + \dfrac{\partial F}{\partial k} - \omega_1 \dfrac{\partial^2\mathscr{D}_0}{\partial k\partial\omega}}{\dfrac{\partial^2\mathscr{D}_0}{\partial k^2}}\right]_{k=k_0,\ \omega=\omega_0}. \tag{A 5}$$

Given that $k = k_0$ is a genuine pinch point, this new saddle point must be one as well; as $|\omega| \to \infty$ we see that $F(k,\omega) \to 0$, and therefore that the movement of the poles in the k-plane as $\mathrm{Im}\,(\omega)$ is increased to large values is determined by the left-hand side of (A 3), and is therefore the same as for the $\epsilon = 0$ case. As we have seen in § 3, it is only for about $\epsilon \geqslant 0.7$ that the assumption that the saddle lies close to (k_0, ω_0) is correct.

REFERENCES

Abrahams, I. D. & Wickham, G. R. 1994 On the stability of a forced elastic surface under a uniformly moving fluid. Paper at EUROMECH 316, Manchester, UK.

Benjamin, T. B. 1960 Effects of a flexible boundary on hydrodynamic stability. *J. Fluid Mech.* **9**, 513–532.

Benjamin, T. B. 1963 The threefold classification of unstable disturbances in flexible surfaces bounding inviscid flows. *J. Fluid Mech.* **16**, 436–450.

Bers, A. 1983 Space-time evolution of plasma instabilities – absolute and convective. In *Handbook of Plasma Physics* (ed. M. N. Rosenbluth & R. Z. Sagdeev), vol. 1, pp. 451–517. North-Holland.

Brazier-Smith, P. R. & Scott, J. F. 1984 Stability of fluid flow in the presence of a compliant surface. *Wave Motion* **6**, 547–560.

Briggs, R. J. 1964 *Electron-stream Interaction with Plasmas*. Monograph No. 29. MIT Press.

Cairns, R. A. 1979 The role of negative energy waves in some instabilities of parallel flows. *J. Fluid Mech.* **92**, 1–14.

Carpenter, P. W. & Garrad, A. D. 1985 The hydrodynamic stability of flow over Kramer-type compliant surfaces. Part 1. Tollmien-Schlichting instabilities. *J. Fluid Mech.* **155**, 465–510.

Carpenter, P. W. & Garrad, A. D. 1986 The hydrodynamic stability of flow over Kramer-type compliant surfaces. Part 2. Flow-induced surface instabilities. *J. Fluid Mech.* **170**, 199–232.

Crighton, D. G. & Oswell, J. E. 1991 Fluid loading with mean flow. I. Response of an elastic plate to localized excitation. *Phil. Trans. R. Soc. Lond.* **335**, 557–592.

Drazin, P. G. & Howard, L. N. 1962 The instability to long waves of unbounded parallel inviscid flow. *J. Fluid Mech.* **14**, 257–283.

Drazin, P. G. & Reid, W. H. 1981 *Hydrodynamic Stability*. Cambridge University Press.

Golubev, V. V. & Atassi, H. M. 1997 Acoustic–vorticity moes in an annular duct with mean vortical swirling flow. *AIAA Paper* 97-1695-cp.

Healey, J. J. 1998 Characterizing boundary-layer instability at finite Reynolds numbers. *Eur. J. Mech.* B/*Fluids* **17**, 219–237.

Junger, M. C. & Feit, D. 1986 *Sound, Structures, and Their Interaction*. MIT Press.

Kelbert, M. & Sazonov, I. 1996 *Pulses and Other Wave Processes in Fluids*. Kluwer.

Landahl, M. T. 1962 On the stability of a laminar incompressible boundary layer over a flexible surface. *J. Fluid Mech.* **13**, 609–632.

Leib, S. J. & Goldstein, M. E. 1986 The generation of capillary instabilities on a liquid jet. *J. Fluid Mech.* **168**, 479–500.

Lighthill, M. J. 1960 Studies on magnetohydrodynamic waves and other anisotropic wave motions. *Phil. Trans. R. Soc. Lond.* **252**, 397–430.

Lin, C. C. 1955 *Hydrodynamic Stability*. Cambridge University Press.

Lingwood, R. J. 1995 Absolute instability of the boundary layer on a rotating disk. *J. Fluid Mech.* **299**, 17–33.

Lingwood, R. J. 1997 On the application of the Briggs' and steepest-descent methods to a boundary-layer flow. *Stud. Appl. Maths* **98**, 213–254.

Lucey, A. D. 1998 The excitation of waves on a flexible panel in a uniform flow. *Phil. Trans. R. Soc. Lond.* **356**, 2999–3039.

Lucey, A. D. & Carpenter, P. W. 1992 A numerical simulation of the interaction of a compliant wall and inviscid flow. *J. Fluid Mech.* **234**, 121–146.

Lucey, A. D. & Carpenter, P. W. 1993 On the difference between the hydroelastic instability of infinite and very long compliant panels. *J. Sound Vib.* **163**, 176–181.

Olendraru, C., Sellier, A., Rossi, M. & Huerre, P. 1996 Absolute/convective instability of the Batchelor vortex. *C. R. Acad. Sci.* IIb **323**, 153–159.

Peake, N. 1997 On the behaviour of a fluid-loaded cylindrical shell with mean flow. *J. Fluid Mech.* **338**, 387–410.

Wu, S. F. & Maestrello, L. 1995 Responses of finite baffled plate to turbulent flow excitation. *AIAA J.* **33**, 13–19.

Yeo, K. S. & Dowling, A. P. The stability of inviscid flows over passive compliant walls. *J. Fluid Mech.* **183**, 265–292.